Applied Catalysis B: Environmental 163 (2015) 214–222

Contents lists available at ScienceDirect

Applied Catalysis B: Environmental

journal homepage: www.elsevier.com/locate/apcatb

Evolution of H_2 photoproduction with Cu content on CuO_x-TiO_2 composite catalysts prepared by a microemulsion method

A. Kubacka [a], M.J. Muñoz-Batista [a], M. Fernández-García [a,*], S. Obregón [b], G. Colón [b,**]

[a] Instituto de Catálisis y Petroleoquímica, CSIC, Marie Curie 2, 28049 -Madrid, Spain
[b] Instituto de Ciencia de Materiales de Sevilla, Centro Mixto CSIC-Universidad de Sevilla, C/Américo Vespucio, 49, 41092 Sevilla, Spain

ARTICLE INFO

Article history:
Received 30 May 2014
Received in revised form 28 July 2014
Accepted 2 August 2014
Available online 12 August 2014

Keywords:
H_2 production
Copper
Titania
Doping
Surface species

ABSTRACT

Copper oxides in contact with anatase correspond to promising materials with high activity in the photoproduction of hydrogen by aqueous reforming of alcohols. By a single pot microemulsion method we obtained a series of Cu–Ti composite systems with controlled copper content in the 0–25 wt.% range. The scanning of such a wide range of composition led to the discovery of two well differentiated maxima in the photo-reaction performance. These maxima present rather high and relatively similar reaction rates and photonic efficiencies but are ascribed to the presence of different copper species. A multitechnique analysis of the materials indicates that the maxima obtained comes from optimizing different steps of the reaction; while the first would be connected with a positive effect on anatase charge handling performance the second seems exclusively related to electron capture by surface copper species.

1. Introduction

Hydrogen is foreseen as one of the most promising energy vectors of the future, providing both high energy efficiency and low greenhouse gas emissions. Current hydrogen technologies rely on several petrochemical related routes among which the reforming of natural gas is the most important [1]. Within the framework of a more sustainable economy and society better solutions are urgently needed and seek. A modern alternative is the photoreforming reaction of alcohols [2–6].

Titania is possibly the most prominent photocatalytic material. Titania-based photocatalysis has significant advantages over traditional technologies as its action is typically carried out under energy efficient conditions, e.g. room temperature and atmospheric pressure [4,7]. However, when titania is utilized in hydrogen production using a photoreforming reaction, a number of factors related to the large overpotential for H_2/O_2 evolution, fast rate of both charge recombination and the back reaction of water formation from the two products make its application unpractical [8,9]. This problem has been tackle with the presence of additional components in TiO_2-based systems. Among the potential options, the use of Pt, Pd, Au, Ni and Cu has shown promising activity. Although noble metals have been profusely investigated [10–15], the use of non-noble metals seems a more robust solution from an economical point of view if adequate activity is achieved. In this context, the use of copper has attracted increasing attention in recent years [16–27].

Copper oxides, Cu_2O and CuO, are photoactive materials with adequate band gap and band edge positions for photowater splitting or reforming [4,6,7]. Unfortunately, they are unstable due to facile photocorrosion in reaction conditions. The interaction with TiO_2 is however a procedure to stabilize the copper oxides and besides, can boost their activity by providing the most efficient light to charge converter known. The adequate band positioning ensures charge transfer and separation between the Cu and Ti phases and the subsequent fostering of the activity [4,6,7].

In this contribution we aim to investigate the CuO_x–TiO_2 composite system within a broad perspective. Specifically, we carried out an analysis of the hydrogen production photocatalytic performance using a set of samples with copper content in the 0–25 wt.% range and found the unexpected presence of two well differentiated maxima corresponding to different copper active species. We investigated the photoreforming activity of Cu–Ti composite samples with methanol as it is foreseen a key energy vector of the future. This would come from the implementation of new low pressure/temperature technologies aiming to control global warming and produce the alcohol from both low and high carbon dioxide concentration sources through the photoelectrochemical reduction of CO_2 using novel enzymatic or inorganic catalysts [28,29].

* Corresponding author. Tel.: +34 915 85 54 75; fax: +34 915 85 47 60.
** Corresponding author. Fax: +34 915 85 47 60.
E-mail addresses: mfg@icp.csic.es, m.fernandez@icp.csic.es (M. Fernández-García), gcolon@icmse.csic.es (G. Colón).

http://dx.doi.org/10.1016/j.apcatb.2014.08.005
0926-3373/

2. Experimental

2.1. Catalyst preparation

Materials were obtained by means of a microemulsion preparation method utilizing *n*-heptane (Scharlau) as organic media, Triton X-100 (Aldrich) as surfactant and hexanol (Aldrich) as cosurfactant. A TiO_2 reference sample was obtained as a first step using a water in oil microemulsion and titanium tetraisopropoxide as precursor. In all composite samples hexahydrated copper nitrate (Aldrich) was used as precursor of the corresponding phase. Water/M (M = Cu, Ti) and water/surfactant molar ratios were, respectively, 110 and 18 for all samples [30,31]. After stirring for 30 min, the stoichiometric quantity of monohydrate hydrazine (Aldrich) for Cu(II) to Cu(0) reduction was introduced from the aqueous phase of a similar microemulsion under stirring for ca. 5 min. Subsequently and for nanocomposite samples, a titanium tetraisopropoxide solution with isopropanol (2:3) was added dropwise on the Cu-containing microemulsion. The resulting mixture was stirred for 24 h, centrifuged, and the separated solid precursors rinsed with methanol and dried at 110 °C for 12 h. After drying, the solid precursors were subjected to a heating ramp (2 °C min^{-1}) up to 450 °C, maintaining this temperature for 2 h. Samples names are Ti or TiO_2 for the reference material and *x*Cu for the composite ones where *x* is the weight percentage content of CuO.

2.2. Experimental techniques

Chemical analysis of the samples was carried out using the total reflection X-ray Fluorescence technique with a TXRF 8030c FEI instrument equipped with a double monochromator. The BET surface areas and average pore volume and sizes were measured by nitrogen physisorption (Micromeritics ASAP 2010).

The X-ray source for X-ray diffraction experiments was Cu Kα radiation (0.15406 nm). Rietveld analyses were performed by using XPert HighScore Plus software over selected samples. Internal reference systems (Si) were used to calibrate the spectrometer. The diffraction patterns were recorded from 2θ 10° to 120° with step of 0.017° and 400 s per step. Crystallite sizes were obtained from Rietveld refinement using silica as internal standard.

UV–vis spectra (Shimadzu, AV2101) were recorded in the diffuse reflectance mode (*R*) and transformed to a magnitude proportional to the extinction coefficient (*K*) through the Kubelka–Munk function, *F*(R1). Samples were mixed with $BaSO_4$ that does not absorb in the UV–vis radiation range (white standard). Scans range was 240–800 nm.

Electron paramagnetic resonance (EPR) spectra were recorded at 77 K with a Bruker ER 200 D spectrometer operating in the X-band and calibrated with a DPPH standard (*g* = 2.0036). Portions of about 30 mg of sample were placed inside a quartz probe cell with greaseless stopcocks using a conventional high vacuum line (capable of maintaining a dynamic vacuum of ca. 6×10^{-3} N m^{-2}) for treatment.

XPS data were recorded on 4×4 mm^2 pellets, 0.5 mm thick, prepared by slightly pressing the powered materials which were outgassed in the prechamber of the instrument at room temperature up to a pressure $<2 \times 10^{-8}$ to remove chemisorbed water from their surfaces. The SPECS spectrometer main chamber, working at a pressure $<10^{-9}$ torr, was equipped with a PHOIBOS 100 multichannel hemispherical electron analyzer with a dual X-ray source working with Mg Kα ($h\nu$ = 1253.6 eV) at 120 W, 20 mA using C 1s as energy reference (284.6 eV). Surface chemical compositions were estimated from XP-spectra, by calculating the integral of each peak after subtraction of the "S-shaped" Shirley-type background using the appropriate experimental sensitivity factors using UNIFIT 2012 software.

Table 1
Copper content and main morphological parameters of the samples.

Samples	Cu content wt.%	BET area (m^2 g^{-1})	Pore volume (cm^3 g^{-1})	Pore size (nm)
Ti	–	69.4	0.113	6.55
0.75Cu	0.7	92.1	0.144	6.28
1.5Cu	1.4	92.7	0.141	6.09
3.0Cu	2.9	78.1	0.123	6.32
4.5Cu	4.7	77.0	0.120	6.37
6.5Cu	6.3	74.4	0.120	6.48
10Cu	9.7	70.2	0.120	6.81
13.5Cu	13.8	67.0	0.117	6.99
17Cu	17.3	64.4	0.111	6.87
21Cu	21.5	67.6	0.116	6.91

Temperature programmed reduction (H_2-TPR) experiments were done according to the following experimental conditions using 200 mg of sample. A 5% H_2/Ar (20 mL/min) flow was used as the reducing atmosphere from room temperature up to 700 °C, with a heating rate of 10 °C/min. A thermal conductivity detector (TCD), previously calibrated using CuO, and a mass spectrometer in line with the TCD, calibrated with reference mixtures, were used to detect variations of H_2 concentration, and, in the case of mass spectrometer, to record possible sub-products formation. A cryogenic trap consisting of a gel formed by adding liquid nitrogen to ethanol, in a Dewar flask, was used to prevent water from entering the detector.

2.3. Photo-catalytic production of hydrogen

Photocatalytic H_2 production tests were performed in a flow-reactor system by suspending the powder photocatalysts (1 g/L) in an aqueous solution (300 mL, MeOH/H_2O 1:11 v/v). The reaction media was continuously thermostated at 23–25 °C to prevent any significant evaporation of the sacrificial agent. The catalyst suspension was firstly degassed with an N_2 stream (150 mL/min) for 30 min. After that the N_2 flow was settled at 15 mL/min and stabilized for 15 min. This nitrogen flow was used to displace the hydrogen produced from the photoreactor headspace toward the GC measuring system. Then, the lamp (Hg medium pressure 125 W presenting two main peaks at ca. 325 and 365 nm; irradiance 132 J s^{-1} m^{-2}) was switched on and the effluent gases were analyzed to quantify H_2 production by gas chromatography (Agilent 490 micro GC) using a thermal conductivity detector connected to a Molsieve 5 A and Pora-PLOTQ columns. Initial (for time → 0) and final (time → ∞) reaction rates were estimated by the slope of the corresponding linear extrapolation of the experimental data. They will be used to facilitate the comparison of the catalysts.

3. Results and discussion

Cu loadings determined by X-ray fluorescence were in good agreement with the expected from synthesis conditions (see Table 1). The Cu–Ti composite samples are high surface materials in the 65–90 m^2 g^{-1} interval. Samples are mesostructured materials with rather similar morphological properties in terms of porosity (Table 1).

The XRD diffraction patterns of the samples are presented in Fig. 1 while the Rietveld analysis outcome is summarized in Table 2 and Fig. 2. Note that although anatase pattern corresponding to the $I4_1/amd$ space group is the single visible contribution observed in Fig. 1, the Rietveld analysis uncovers some differences among samples. Most important differences concerning cell tetragonality and volume are plotted in Fig. 2. The differences in the two parameters divide the sample set in two well differentiated groups. In the first, low loading group an increase of the tetragonality accompanied by

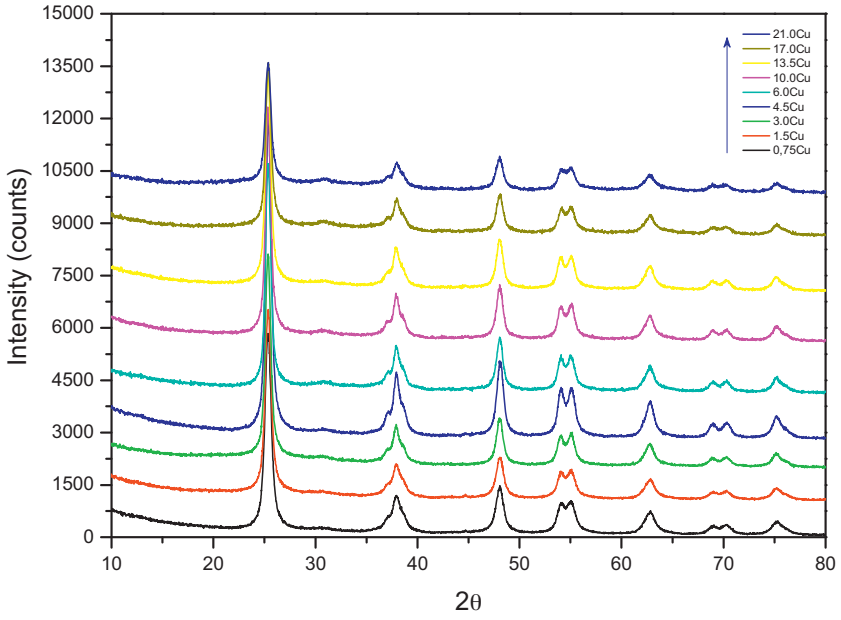

Fig. 1. X-ray diffraction patterns for Cu–Ti composite samples.

a drastic increase in the cell volume are observed. In the second a decreasing tetragonality and moderate raise in the cell volume are detected. This evolution in structural parameters would imply a clear distortion of the anatase unit cell by the incorporation in certain extent of copper ions. Indeed, considering the difference in the ionic radii for Cu^{2+} and Ti^{4+} in octahedral coordination (87 vs. 74 pm, respectively), the observed cell expansion is a strong indication of the Cu incorporation into the anatase structure. In absence of noticeable primary particle size changes producing differential quantum size effects (Table 2) [4], these structural changes are thus interpreted as an effect of doping. Cu doping of titania has been previously analyzed and shown to influence the cell parameters in a similar way to the first group [32]. It would thus indicates that Cu appears to be inserted more effectively into the anatase lattice in samples with copper content below ca. 4.5 wt.%. This insertion effect seems to be reversed at higher loadings, likely as an effect of the preparation conditions, indicating an optimum copper concentration for the doping process. However, as other authors have been already reported, there exists a Cu doping limit of ca. 0.2–0.3% in anatase structure (see below). We attempted to obtain information of this copper species using electron paramagnetic resonance (EPR) but the 0.75 wt.% sample (the lowest loading essayed) is already dominated by a broad, featureless signal ($g_{||} = 2.24$; $g_{\perp} = 2.07$) characteristic of Cu^{2+} ions in dimensionally restricted cluster oxides

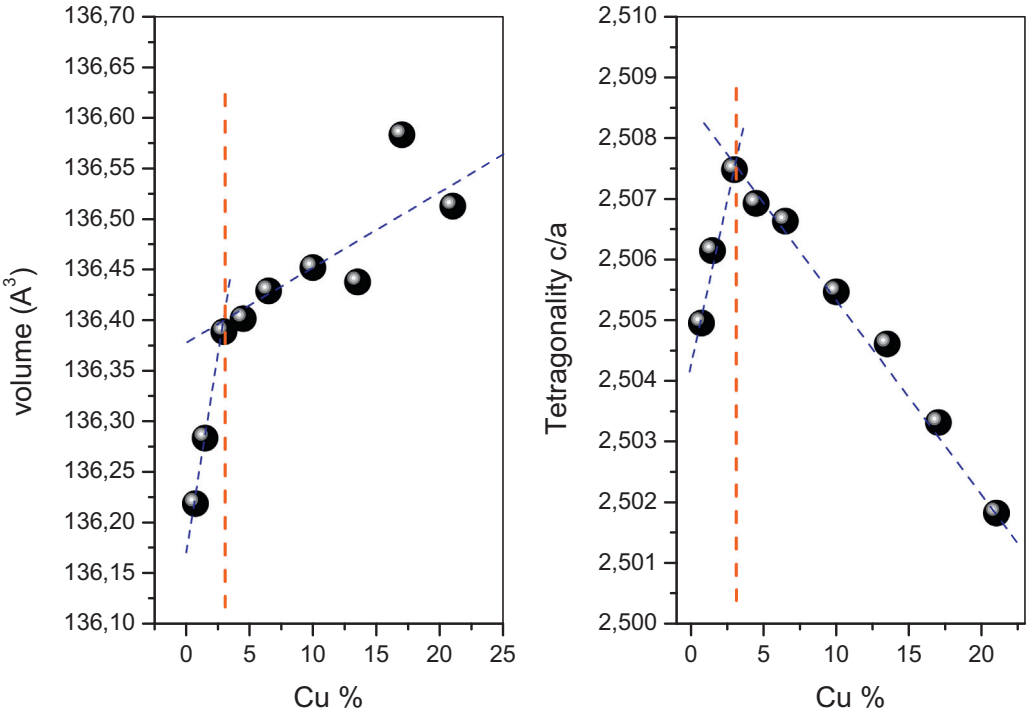

Fig. 2. Cell volume and tetragonality of the anatase phase present in Cu–Ti composite samples.

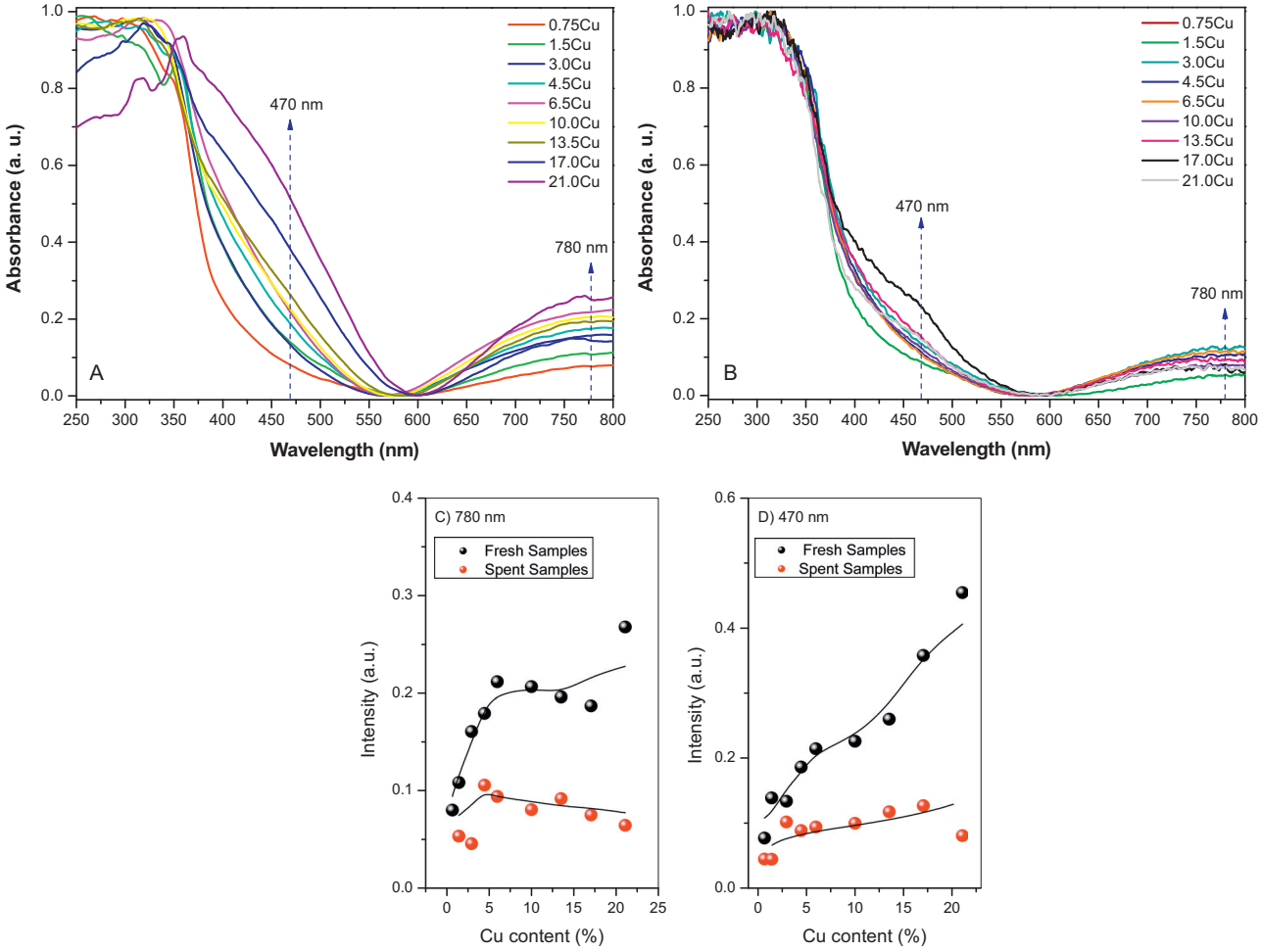

Fig. 3. UV–visible observables for TiO_2 reference and Cu–Ti composite samples. (a) Fresh samples spectra; (b) spent (post-reaction) samples spectra; (c) intensity behavior of the 780 nm contribution; and (d) intensity behavior of the 470 nm contribution.

(result not shown) [33]. The dominance of the aggregated CuO_x cluster in samples with a copper content above 0.5 wt.% is typically observed in the literature [33,34] and only for very low loaded samples, below 0.2 wt.%, the doping copper species is clearly detected. The result suggests that for low loading samples, the doping copper species is a relatively minor species which however grows with the copper content (a maximum of ca. 0.2–0.3 wt.% is expected). The majorly of copper is thus forming a XRD-silent, amorphous and/or size restricted CuO_x phase.

Further analysis of the copper species was carried out with the help of UV–visible spectroscopy. Fig. 3 displays the corresponding spectra. They are dominated by the anatase band gap with two additional features. The first one is centered at ca. 470 nm and is ascribed to copper species present into a CuO matrix [35]. The second is located at ca. 780 nm and ascribed to the E_g to T_{2g} electronic transition at Cu^{2+} ions with distorted octahedral geometry caused by a Jan–Teller effect [36,37]. Thus two additional copper species to the one located at the anatase lattice are present. The first corresponds to Cu^{2+} ions at dimensionally restricted CuO_x clusters and having the usual square planar symmetry [37–39]. The second are isolated or nearly isolated (i.e. oligomers) species located at the anatase surface which provides the adequate environment for a distorted octahedral geometry, not typical of copper oxides. Note that CuO_x cluster even with restricted dimensionality are relatively poor

Table 2
Rielveld results obtained from XRD pattern analysis of the anatase phase present in Cu–Ti composite samples and TiO_2 reference.

Sample	Anatase cell paramters (nm)		Volume (nm^3)	c/a	Size (nm)
	$a=b$	c			
Ti	3.784	9.468	135.6	2.502	11.2
0.75Cu	3.789	9.490	136.2	2.505	12.1
1.5Cu	3.789	9.495	136.3	2.506	12.5
3.0Cu	3.788	9.497	136.3	2.507	14.0
4.5Cu	3.789	9.499	136.4	2.507	14.1
6.5Cu	3.790	9.499	136.4	2.506	14.2
10.0Cu	3.790	9.497	136.4	2.505	14.8
13.5Cu	3.791	9.494	136.4	2.504	14.9
17Cu	3.793	9.495	136.6	2.502	14.6
21Cu	3.793	9.489	136.5	2.502	14.2

Table 3
XPS results for selected smaples.

Sample		Cu^{+}		Cu^{2+}		Im/Is[a]	Cu/Ti
		B.E. (eV)	at.%	B.E. (eV)	at.%		
3Cu	Fresh	932.2	92	933.4	8	12.7	0.088
	Post	932.2	87	933.5	13	7.4	0.086
10Cu	Fresh	932.4	79	934.1	20	9.7	0.192
	Post	932.5	68	934.1	32	6.5	0.191
13.5Cu	Fresh	932.2	67	933.5	33	6.3	0.207
	Post	932.2	56	933.7	44	4.8	0.196

[a] The intensity ratio of main peak and satellite peak.

and, more importantly, non stable hydrogen production systems [38,39].

In Fig. 3C and D we show the intensity behavior of the above mentioned 780/470 nm bands in fresh and used samples. Copper doping of the anatase structure is known to produce a relatively mild effect in titania band gap (less than 0.2–0.3 eV) [36] allowing the easy following of the copper species evolution in the sample series due to the limited effect of changes in band gap position. First to mention is the fact that due to the different absorption coefficient of these two components as well as the presence of optically silent

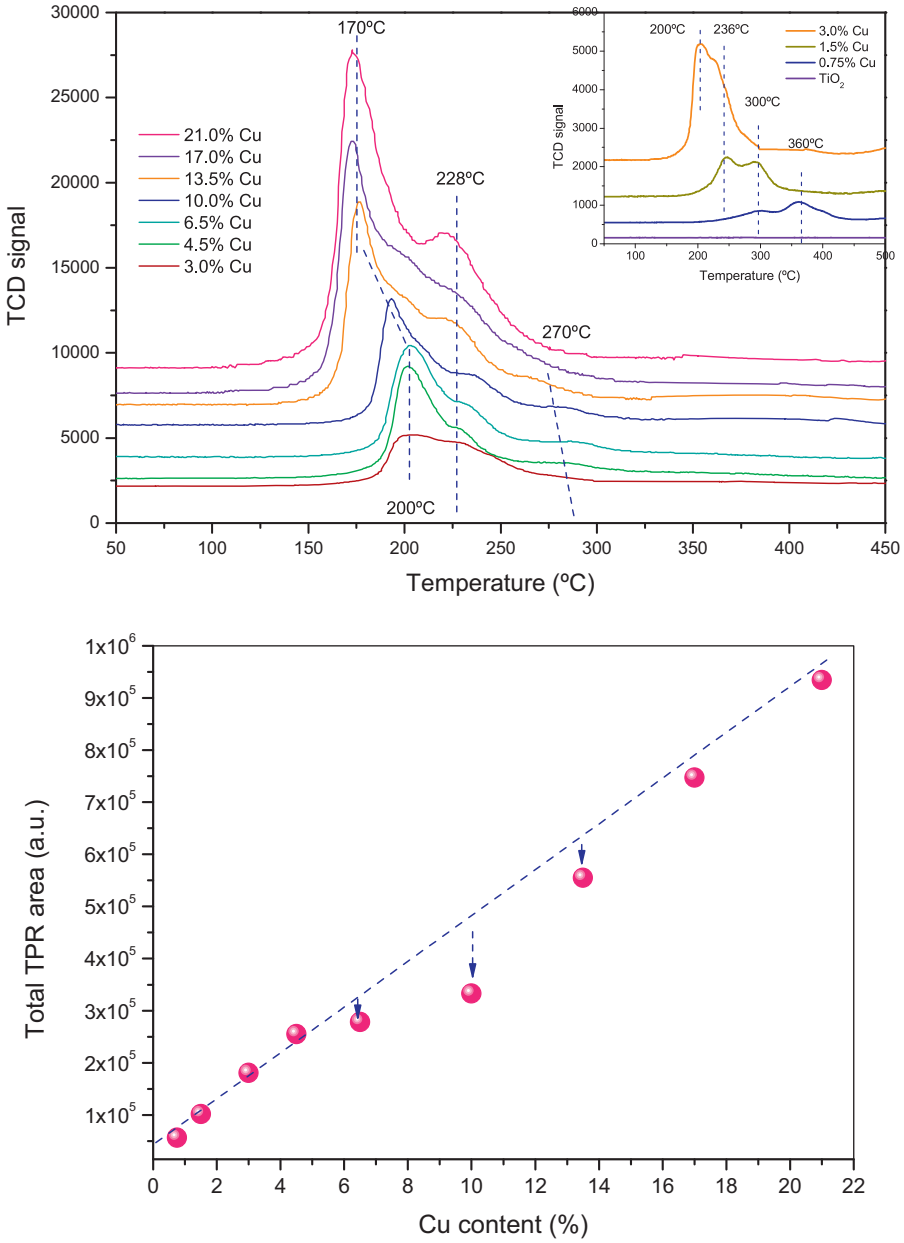

Fig. 4. TPR profiles for Cu–Ti composite samples (upper panel) and integration of the signal (lower panel).

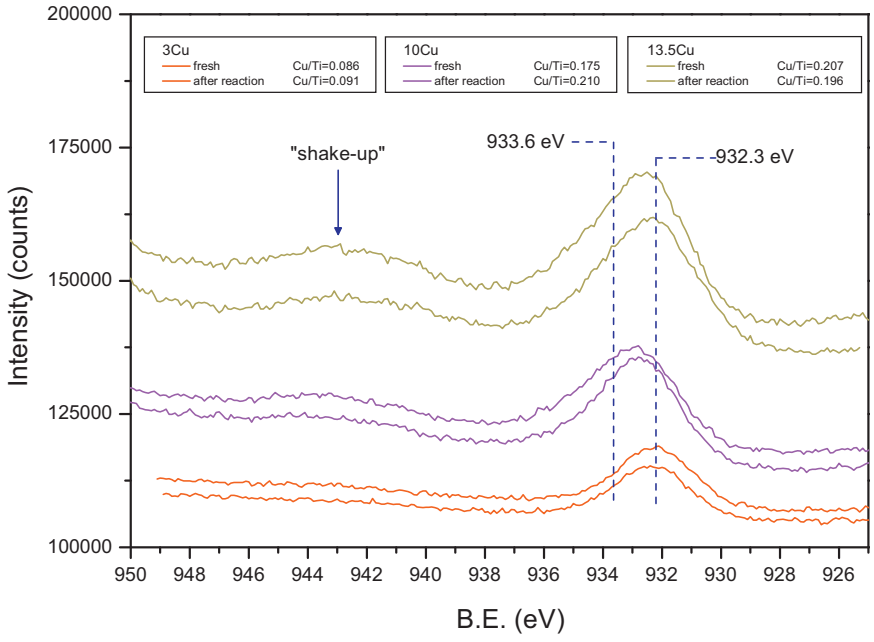

Fig. 5. X-ray photoelectron spectra for selected Cu–Ti composite samples.

species (as the doping ions), the intensity of these two bands does not provide information concerning the importance of each species to the copper distribution [36,37]. We can also mention that while the absolute intensity varies between these two series (fresh and spent – post-reaction – samples) by an effect of several physico-chemical variables including the evolution of the copper species (in this respect note that copper losses during reaction would be relatively small according to XPS measurements of fresh and used samples – see Table 3), the trend observed vs. the copper content is reasonably similar in fresh and spent samples. In both Fig. 3(C and D) we consistently observe two regions of behavior, above and below ca. 3.0 wt.% Cu. Although this is more clearly observed in the fresh samples, the limit is broadly consistent with that detected by XRD in Fig. 2 and would thus provide further evidence that a different copper distribution below and above the turning point detected in all figures. Such turning point affects all copper species, i.e. doped or surface related entities.

In order to test their reducibility we carried out a temperature programmed reduction in hydrogen (TPR). Fig. 4 (upper panel) presents the experimental results. Several peaks are observed in the hydrogen consumption profile. Low temperature peaks, at ca. 170, 200 and 230 °C, identify three different species assigned to copper oxide clusters with variable dimensions as reduction of such species occurs in a single step as far as the technique can see. In fact the last two peaks are typical of well developed CuO clusters [40]. We stress that such CuO-type species are amorphous-like according to XRD (Fig. 1). The set of 170–230 °C peaks dominates the TPR profile of the high loading samples (Fig. 4). Low loading samples are characterized by peaks located at ca. 300 and 360 °C, that could be associated to copper ions in strong interaction with the titania support [40,41]. Thus, it can be assumed that such species would typically show near octahedral geometry, in agreement with the UV–visible analysis, and their dominant presence at anatase surface or near surface sites [40].

The most interesting point is the integration of the signal, shown in the lower panel of Fig. 4. We observed a linear trend from low loading samples which is recovered only by the high loading sample(s). Starting about 6 wt.%, a lower than expected hydrogen consumption is observed. The linear relationship is however recovered above ca. 13 Cu wt.%. This phenomenon (i.e. the depression region observed for middle copper content from the linear behavior presented in Fig. 4 as a dotted line) likely indicates the presence of non reducible copper species (at temperatures below 400 °C) by strong interaction with the support. As shown by XPS (Table 3 and Fig. 5) the alternative interpretation based exclusively in a different Cu^{+}/Cu^{2+} ratio though the samples series is not possible as we did not observe the same (hypothetical) Cu^{+}/Cu^{2+} trend(s) vs. copper content for TPR and XPS signals. The XPS variation through the sample series is at odds with the TPR one as it shows a somewhat monotonic increase with the copper content which would result in a different behavior than the one presented in Fig. 3. This is likely due, at least in part, to the in-situ reduction of copper species with low interaction with the support at the XPS measurement conditions. The latter has been previously observed in numerous Cu–Ti systems [35,42]. We can also dismiss a variable contribution of a potential co-reduction of anatase, which seems rather limited in the range of temperatures scanned, as would be expected from the result of the pure reference system (shown in Fig. 4) as well as from results presented in previous publications [40].

The joint analysis of XRD-Rietveld, UV–visible, TPR, EPR and XPS measurements indicates that a significant number of copper species are present in the materials; the number and physico-chemical properties of such phases being dependent on the copper loading. The multitechnique approach provides evidence of copper ions at anatase lattice positions, several copper ions or oligomer species sited at the surface of anatase, and CuO-like clusters of different dimensionality, being detected for the latter at least two types, those with a reduction behavior relatively close/far from bulk CuO [16–32]. The heterogeneity of copper in the composite system is thus a constant even from low loading samples and indicates the relatively low quality information that would come from other atom-averaged techniques like X-ray absorption, which will provide little fine details even for our lowest copper weighted sample. At the same time, Table 1 indicates that the titania counterpart is relatively similar in all materials (see for example, the primary particle size and porosity) expect in properties related to doping by copper.

The activity of the materials in hydrogen evolution is presented in Fig. 6. We tested the activity for a total of 16 h at a controlled

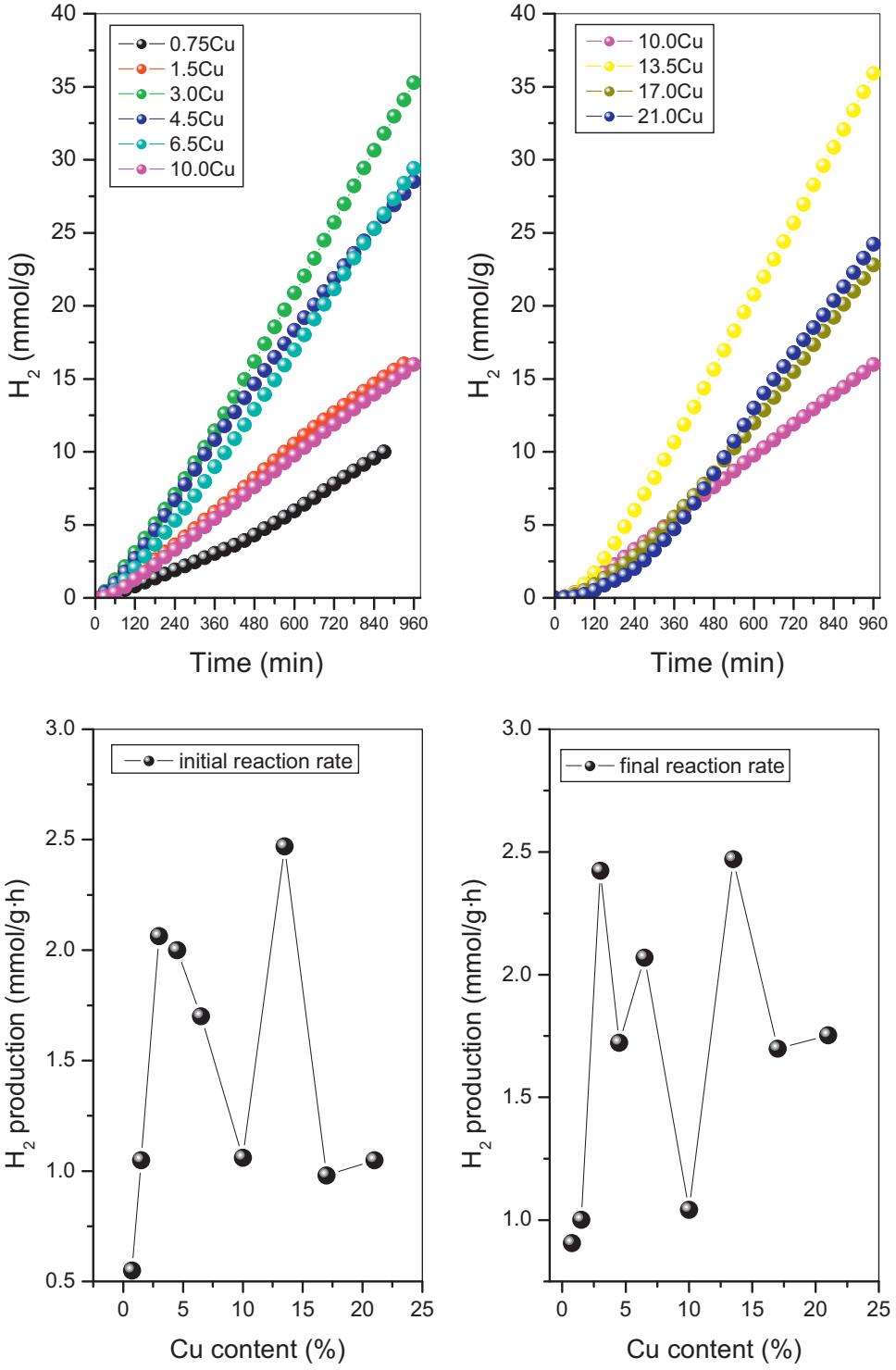

Fig. 6. Photocatalytic results for hydrogen production: upper panel; time on stream data; lower panel; initial and final reaction rates.

temperature of ca. 25 °C, indicating the reasonable stability of the system under reaction conditions. Samples display different behaviors from the beginning of the reaction, with presence of an induction period in some cases where activity is poor (for example, 0.75Cu, 17Cu and 21Cu). This may indicate copper evolution in such samples. More importantly, the presence of two well defined maxima of activity vs. copper content is immediately spot out. The two samples showing optimum activity display a relatively similar reaction rate per gram of material (2.07 vs. 2.48 mmol g^{-1} h^{-1} for, respectively, 3.0 and 13.5 wt.% Cu samples). As far as we know this is the first time this behavior is uncovered and reported. The first maximum is located in the copper content zone below ca. 6 wt.% and shows a marked parallelism with the behavior of the cell tetragonality presented in Fig. 2. The only copper species envisaged to provide this behavior is the copper ions located at the anatase lattice. The importance of this species in hydrogen photoproduction has been mentioned in previous reports [26]. Such copper species is expected to modify the bang gap for a limited amount as well as to alter charge carrier recombination. Due to the limited effect expected for a band gap change in absorption properties due to the

nature of our UV source (with very low intensity above 380 nm) the second seems potentially more important.

The high copper concentration maximum is more complex to analyze due to the higher structural complexity of the composite materials [21]. Nevertheless, the two singular copper species present in the high loading samples are: (i) large CuO-type clusters, as previously mentioned poorly active [38,39,43], and (ii) the surface copper species, likely related to ions/oligomers strongly stabilized by interface contact with the titania phase. Among the second class of species, the only one presenting a reasonable similitude (i.e. behavior though the sample series) with the photoactivity behavior observed after the first maximum (Fig. 6) would be the non-reducible species detected in the TPR experiment. We can also note that a region of high activity for highly loaded copper loaded samples has been envisaged by Sun and coworkers [39].

According to the multitechnique characterization, we can thus conclude that two copper species in a Cu^{2+} state may be determinant in driving photoactivity along the Cu–Ti sample series. The first, the doping copper ions at anatase lattice positions, is likely related to improve the charge handling aspect(s) within the titania phase while the second, strongly interacting copper species at the surface of the anatase phase, would be the most efficient in (multi)-electron capture processes [2,9]. It is unlikely that these species suffer a (stable) reduction process during reaction but might be possible in the later case (XPS – Table 3 – may indicate this although, as previously mentioned, the result is inconclusive in this respect and, moreover, the TPR result would indicate the non-reducibility of the species). Again, we note that due to the inherent heterogeneity of the samples what we call strongly interacting copper species is in fact a family of copper species (all of them located at surface or near surface positions of the titania and having pseudo-octahedral symmetry according to their optical features) which can be further differentiated but this is not possible with current physico-chemical techniques. Interesting to note is that the two maxima can be obtained using the same preparation method.

We finally stress that the maximum rate achieved and expressed per gram of catalyst is in our case of the same order of magnitude to those reported for noble metals [10–15]. Moreover if we consider the relatively low concentration of the active copper species, the real rate is significantly higher. A rough estimation of the copper concentration at the two maxima indicates that the low/high copper concentration maxima can be multiplied by more than 10/5 times assuming the estimation of the first/second species "partial" percentage as extracted from, respectively, the EPR and TPR studies. Although these are, as mentioned, very rough estimations, they would indicate that the first species is more efficient than the second. We also calculated the photonic efficiency (as the moles per second of hydrogen produced divided by the moles of photons – Einsteins – per second) [44] for the two materials providing the largest reaction rates. Without any correction which would take into account the different copper species, we obtained a photonic efficiency of 8.9 and 10.7% for, respectively, the samples having 3.0 and 13.5 wt.% of copper. Such numbers can be compared favorably with those obtained with catalysts containing noble metals [10–15,45] as well as copper [16–26] (typically below 35% in the case of noble metals) and indicates the goodness of the systems here studied.

4. Conclusions

In this contribution we synthesized a series of Cu-Ti composite catalysts by a single pot microemulsion method followed by calcination at 450 °C. The preparation method yielded high surface area, mesoporous materials and having control of the copper content in the 0–25 wt.% interval.

The Cu–Ti composite samples were tested in the photoreforming of methanol. The sample series displays a non classical behavior with presence of two well differentiated maxima corresponding to samples having a 3.0 and 13.5 wt.% of copper. The physico-chemical characterization identifies two different copper species as responsible of the activity maxima. While both are fully oxidized species, they are structurally different and likely influence activity in very different ways. We propose that the first is a doping agent at the anatase lattice which would influence charge handling properties within such phase. The second is a non-reducible (during a TPR at moderate temperatures) oxidized species with local geometry indicating its location in or near by the anatase surface. The reaction rates observed are relatively similar, moderately favoring the second species, although a rough estimation of the specific activity per single site may in fact indicate that the first species is intrinsically more active. The analysis of the photonic efficiency also provides evidence of the goodness of the system, with a maximum value near 10.7%. Finally, it is worth to mention that the results here presented indicate that the intensification of the hydrogen photoproduction process over the Cu–Ti system may be approached through two independent ways and thus could be optimized significantly by adequate material engineering procedures.

Acknowledgments

A. Kubacka and M.J. Muñoz-Batista thank Spanish MINECO for, respectively, Raman y Cajal Post-doctoral and FIP Predoctoral fellowships. S. Obregón also thanks CSIC for the concession of a JAE-Pre grant. The financial support by projects ENE2013-46624-C4-1-R, *P09-FQM-4570*, and *ENE2011-24412* is fully acknowledged.

References

[1] R. Smith, N. Zhang, J. Zhao, Chem. Eng. Trans. 29 (2012) 1099–1104.
[2] A. Kudo, Y. Misaki, Chem. Soc. Rev. 38 (2009) 253–278.
[3] K. Maeda, J. Photochem. Photobiol. C 12 (2011) 237–268.
[4] A. Kubacka, M. Fernández-García, G. Colón, Chem. Rev. 112 (2012) 1555–1614.
[5] A. Iwasa, H. Kato, A. Kudo, Appl. Catal. B 136–137 (2013) 89–93.
[6] J. Yang, D. Wang, H. Han, C. Li, Acc. Chem. Res. 46 (2013) 1900–1909.
[7] L. Jing, W. Zhou, G. Tian, H. Fu, Chem. Soc. Rev. 42 (2013) 9509–9549.
[8] D.Y.C. Leung, X. Fu, C. Wang, M. Ni, M.K.H. Leung, ChemSusChem 3 (2010) 681–694.
[9] Y. Qu, X. Duan, Chem. Soc. Rev. 42 (2013) 2568–2580.
[10] T. Srethawrong, Y. Suzuki, S. Yoshikawa, Int. J. Hydrogen Energ. 30 (2005) 1053–1062.
[11] Q. Xu, Y. Ma, J. Zhang, X. Wang, Z. Feng, C. Li, Int. J. Hydrogen Energ. 33 (2008) 1243–1251.
[12] V.M. Daskalaki, D.I. Kondarides, Catal. Today 144 (2009) 75–80.
[13] Q. Gu, X. Fu, X. Wang, S. Chen, D.Y.C. Leung, X. Xie, Appl. Catal. B 106 (2011) 1243–1251.
[14] A. Gallo, T. Montini, M. Marelli, A. Minguzzi, V. Gombac, R. Psaro, P. Fornasiero, V. del Sarto, ChemSusChem 5 (2012) 1800–1811.
[15] S. Obergón, G. Colón, Appl. Catal. B 144 (2014) 775–782.
[16] Y.S. Chaudhary, A. Agrawal, R. Shivastav, V.R. Satsangi, S. Dass, Int. J. Hydrogen Energ. 29 (2004) 131–134.
[17] Y. Wu, G. Lu, S. Li, Catal. Lett. 133 (2009) 97–105.
[18] T. Miwa, S. Kaneco, H. Katsumata, T. Suzuki, K. Ohta, S.C. Verma, K. Sugihara, Int. J. Hydrogen Energ. 35 (2010) 6554–6560.
[19] K. Lalitha, G. Sudanandam, V.D. Kumari, M. Subrahmanyan, B. Sreedhar, N.Y. Heblakar, J. Phys. Chem. C 114 (2010) 22181–22189.
[20] V. Gombac, L. Sordelli, T. Montini, J.J. Delgado, A. Adamski, G. Adami, M. Cargnello, S. Bernal, P. Fornasiero, J. Phys. Chem. A 114 (2010) 3916–3925.
[21] S. Xu, A.J. Du, J. Liu, J. Ng, D.D. Sun, Int. J. Hydrogen Energ. 36 (2011) 6560–6568.
[22] M. Liu, X. Qiu, M. Miyauchi, K. Hashimoto, Chem. Mater. 23 (2011) 5282–5286.
[23] S.L. In, D.D. Vaughn, R.E. Shaack, Angew. Chem. Int. Ed. 51 (2012) 3915–3918.
[24] D.W. Skaf, N.G. Natrin, K.C. Brodwater, C.R. Bongo, Catal. Lett. 142 (2012) 1175–1179.
[25] Y. Fang, R. Wang, G. Jiang, H. Jin, Y. Wang, X. Sun, S. Wang, T. Wang, Bull. Mater. Sci. 35 (2012) 495–499.
[26] C. Ampelli, R. Passalacqua, C. Genovese, S. Perathorner, G. Centi, T. Montini, V. Gombac, J.J. Delgado, P. Fornasiero, RSC Adv. 3 (2013) 21776–21788.
[27] D.P. Kumar, M.V. Sankar, M.M. Kumari, G. Sadanandam, B. Srinivas, V. Durgakumari, Chem. Commun. 49 (2013) 9443–9947.
[28] T.W. Woolerton, S. Sherad, E. Pierce, S.W. Regshale, Energy Environ. Sci. 4 (2011) 2393–2399.

[29] F. Studt, I. Sarafultinov, F. Abild-Petersen, C. Felkjaer, J.S. Hummerlshoj, S. Dahl, I. Chorkendroff, J.K. Norskov, Nat. Chem. (2014), http://dx.doi.org/10.1038/Nchem.1873.
[30] P.G. De Gennes, C. Taupin, J. Phys. Chem. 86 (1982) 2294–2303.
[31] A. Kubacka, G. Colón, M. Fernández- García, Catal. Today 143 (2009) 286–292.
[32] N. Lock, E.M.L. Jensen, J. Mi, A. Mamakhel, K. Nosen, M. Quigbo, B.B. Iversen, Dalton Trans. 42 (2013) 9555–9564.
[33] G. Li, N.M. Dimitrijevic, L. Chen, T. Rajh, K.A. Gray, J. Phys. Chem. C 112 (2008) 19040–19044.
[34] A. Martínez-Arias, A.B. Hungría, M. Fernández-García, J.C. Conesa, J. Soria, J. Phys. Chem. B 104 (2004) 17983–17991.
[35] G. Colón, M. Maicu, M.C. Hidalgo, J.A. Navío, Appl. Catal. B 67 (2006) 41–51.
[36] R. Khan, S. Wkima, T.-J. Kim, J. Nanosci. Nanotechnol. 10 (2010) 983–987.
[37] J.J. Bravo-Suárez, B. Subramaniam, R.V. Chaudhari, J. Phys. Chem. C 116 (2012) 18207–18221.
[38] C.-H.- Kuo, M.H. Huan, Nano Today 5 (2010) 106–116.
[39] S. Xu, J. Ng, X. Zhang, H. Bai, D.D. Sun, Int. J. Hydrogen Energ. 35 (2010) 5254–5261.
[40] H. Zhu, L. Dong, Y. Chen, J. Colloid. Inter. Sci. 357 (2011) 497–503.
[41] J.Y. Kim, J.A. Rodriguez, J.C. Hanson, A.I. Frenkel, P.L. Lee, J. Am. Chem. Soc. 125 (2003) 10684–10692.
[42] A. Kubacka, M. Muñoz-Batista, M. Ferrer, M. Fernández-Garcia, Appl. Catal. B 140–141 (2013) 680–690.
[43] S. Xu, A.J. Du, J. Liu, D.D. Sun, Int. J. Hydrogen Energ. 36 (2011) 6560–6568.
[44] B. Ohtani, Chem. Lett. 37 (2008) 167–189.
[45] S. Strataki, V. Bekhiara, D.I. Kondarides, P. Lianos, Appl. Catal. B 77 (2007) 184–189.